Expert Systems With Applications 272 (2025) 126765

Contents lists available at ScienceDirect

Expert Systems With Applications

journal homepage: www.elsevier.com/locate/eswa

Analyzing bi-objective optimization Pareto fronts using square shape slope index and NSGA-II: A multi-criteria decision-making approach

Bilal H. Al-Majali [a,b], Ahmed F. Zobaa [b,*]

[a] Electrical Engineering Department, Mutah University, Karak, Jordan
[b] Electronic and Electrical Engineering Department, Brunel University of London, Uxbridge, UK

ARTICLE INFO

Keywords:
MCDM
Pareto front
Optimization
Evolutionary algorithms

ABSTRACT

This paper introduces the Square Shape Slope Index (SSSI), a novel post-optimization multi-criteria decision-making (MCDM) approach for analyzing Pareto fronts generated from bi-objective optimization problems. SSSI leverages multiple Utopia and Nadir points—guided by a user-defined priority scale—to form a dynamic square region around particular segments of the Pareto front. Within this region, slope-based evaluations are used to rank solutions based on user preferences and criteria. The method's effectiveness is demonstrated through empirical tests on diverse benchmark functions and real-world scenarios, such as energy distribution and portfolio optimization, each encompassing various shapes and patterns of the Pareto front. In addition, SSSI is compared against established decision-making approaches both geometrically and analytically using different aggregation methods. To account for the stochastic nature of evolutionary algorithms, the Non-Dominated Sorting Genetic Algorithm (NSGA-II) is employed to generate Pareto fronts for each test function. Results confirm the robustness and adaptability of SSSI, offering a clear and flexible framework for balancing conflicting objectives in multi-objective decision-making contexts.

1. Introduction

In multi-objective optimization problems, the objectives often conflict, making multi-objective evolutionary algorithms a common approach. However, these algorithms do not yield a single optimal solution; instead, they produce a set of optimal solutions known as the Pareto front. The core challenge then becomes selecting the most suitable solution from this front, as each solution represents a distinct compromise among objectives (Chiu et al., 2016). This selection process is especially crucial in practical applications, such as optimizing zero-waste food production processes to balance sustainability and efficiency (Capossio et al., 2022). To address this challenge, Multi-Criteria Decision-Makers (MCDMs) serve as essential tools in ensuring that the chosen solution is both technically feasible and optimally aligned with the overarching objectives and constraints (Chaudhuri & Sahu, 2021).

In general, decision-makers follow a series of structured steps. They begin by specifying both the criteria and the alternatives that define the decision problem. In multi-objective optimization contexts, these criteria represent the objectives, while the alternatives correspond to non-dominated solutions (Kaim et al., 2018). Once the decision problem is clearly identified, the decision-maker assigns weights to each objective to reflect its importance, a step that significantly influences the overall outcome. Finally, decision-makers employ various methods to rank the alternatives based on the established criteria.

Based on their decision-making approaches, MCDMs are generally classified into three main categories: Priori, Posteriori, and interactive methods. In the Priori approaches, the decision-maker establishes preferences—including criteria weights—before the optimization process begins, using these preferences to guide subsequent decisions (Wang & Jia, 2020; Syan & Ramsoobag, 2019; Petchrompo & Parlikad, 2019). In contrast, Posteriori approaches define preferences and evaluate non-dominated solutions after the multi-objective optimization process is complete (Petchrompo et al., 2022). Finally, interactive decision-making methods serve as dynamic approaches that engage with the optimization process directly, iteratively refining preferences and evaluating solutions in real time (Fernandez et al., 2018; Fernandez et al., 2020; Nebro et al., 2018).

Compared with Priori and interactive decision-making approaches, Posteriori approaches offer several notable advantages, chiefly because they allow for an analysis of the entire set of alternatives before any preferences are established. Unlike Priori methods, which rely on predefined preferences that may not fully capture the diversity of

* Corresponding author.
E-mail addresses: B.Majali@mutah.edu.jo (B.H. Al-Majali), azobaa@ieee.org (A.F. Zobaa).

https://doi.org/10.1016/j.eswa.2025.126765
Received 10 June 2024; Received in revised form 24 January 2025; Accepted 3 February 2025
Available online 7 February 2025

available solutions, Posteriori approaches expose decision-makers to the actual trade-offs involved, often resulting in more refined and adaptable preference formulation. Furthermore, Posteriori approaches typically demand less computational time for decision-making than interactive methods, since they do not require continuous preference adjustments throughout the optimization process (Petchrompo et al., 2022).

Posteriori decision-making approaches vary widely, with each employing distinct techniques to tackle multi-objective optimization problems. Among these, Euclidean distance–based MCDM methods are foundational, leveraging geometric principles to evaluate alternatives in a multi-dimensional space of criteria (Soheyli et al., 2016). These methods provide intuitive and systematic ways to rank choices. Prominent examples include TOPSIS (Technique for Order of Preference by Similarity to Ideal Solution), which measures the proximity of alternatives to ideal and anti-ideal solutions, and COPRAS (Complex Proportional Assessment), which calculates a proportional utility score by incorporating both beneficial and non-beneficial criteria (Trung, 2021; Taherdoost & Mohebi, 2024). Similarly, VIKOR (VlseKriterijumska Optimizacija I Kompromisno Resenje) emphasizes compromise solutions, ranking alternatives based on their closeness to an ideal solution while considering both group utility and individual regret (Vaid et al., 2022). GRA (Grey Relational Analysis) adopts a relationship-based perspective, comparing alternatives by their closeness to a reference sequence under conditions of uncertainty (Jana & Pal, 2021). MOORA (Multi-Objective Optimization by Ratio Analysis) simplifies decision-making by normalizing criteria and optimizing objectives through additive or ratio-based approaches, enhancing its adaptability across various decision scenarios (Başaran & Tarhan, 2022). Together, these methods effectively address trade-offs among criteria, providing robust and interpretable rankings.

In addition to Euclidean distance-based methods, outranking approaches like PROMETHEE (Preference Ranking Organization Method for Enrichment Evaluation) and ELECTRE (ELimination Et Choix Traduisant la REalité) offer complementary frameworks for decision-making. PROMETHEE employs preference functions and outranking flows to rank alternatives, making it particularly suitable for scenarios involving nuanced preferences (Akram & Bibi, 2023). ELECTRE, on the other hand, uses concordance and discordance indices to assess how one alternative outranks another, accommodating mixed levels of preference and uncertainty (Taherdoost & Madanchian, 2023). Additionally, the Minimum Manhattan Distance (MMD) method emphasizes computational efficiency in identifying solutions closest to ideal outcomes, further enriching the landscape of MCDM techniques (Chiu et al., 2016). Weight determination methods like AHP (Analytic Hierarchy Process) integrate seamlessly with these frameworks, enabling decision-makers to tailor rankings based on specific priorities. Together, these MCDM approaches—including VIKOR's compromise-driven model—serve as powerful tools for solving complex decision-making problems across domains such as renewable energy, logistics, and strategic planning (Doke et al., 2021).

In this paper, we introduce the Square Shape Slope Index (SSSI), a novel Posteriori multi-criteria decision-making (MCDM) method designed specifically for bi-objective optimization problems. The SSSI framework distinguishes itself from existing methods by leveraging multiple Utopia and Nadir points, dynamically adjusting these reference points based on user-defined criteria weights and priorities. Unlike traditional Euclidean distance-based approaches, SSSI employs slope calculations within a dynamic square framework to evaluate and rank alternatives, offering greater adaptability to diverse Pareto front shapes, including convex, non-convex, and discontinuous patterns.

This paper provides a detailed conceptual framework for SSSI, outlining its capacity to balance computational simplicity with decision-making accuracy. To validate its effectiveness, SSSI is compared against well-established posteriori decision makers across various benchmark problems and applied to two real-world case scenarios: energy distribution optimization and portfolio optimization. These applications demonstrate SSSI's practical relevance and ability to handle conflicting objectives in realistic decision-making contexts. Furthermore, we analyze the influence of the stochastic nature inherent in evolutionary algorithms on decision-making processes, showcasing SSSI's ability to maintain consistent performance in the face of optimization variability. These contributions position SSSI as a versatile and innovative tool for addressing complex decision-making challenges in multi-objective optimization.

2. Square shape slop Index (SSSI)

The Square Shape Slope Index (SSSI) is a multi-criteria decision-maker designed for bi-objective optimization problems. It employs the concept of multiple Utopia and Nadir points, governed by a priority scale, to form a square shape around a specific region of the Pareto front. In general, multi-objective optimization can be defined as follows:

$$\begin{matrix} min f(x) \\ x \in \Omega \end{matrix} \tag{1}$$

$$\mathbf{f}(\mathbf{x}) = [\,\mathrm{f}_1(x) \quad \mathrm{f}_2(x) \quad \cdots \quad \mathrm{f}_N(x)\,]^{\mathrm{K}} \tag{2}$$

Where x represents a vector of decision variables in the search space (Ω), while f(x) denotes a set of K objective functions. When an evolutionary algorithm is used to optimize the multi-objective function presented in Eq. (1), it yields a Pareto set S_P. This set consists of all decision vectors x in the feasible decision space Ω for which no other vector x′ in Ω dominates them, as defined in Eq. (3) (G. Cocchi et al., 2021).

$$S_P = \left\{ \mathbf{x} \in \Omega \middle| \forall \mathbf{x}' \in \Omega, \nexists i \in \{1, 2, \cdots, K\} : f_i(\mathbf{x}) < f_i(\mathbf{x}') \text{ and } \forall j \in \{1, 2, \cdots, K\}, f_j(\mathbf{x}) \le f_j(\mathbf{x}') \right\} \tag{3}$$

The image of Pareto set creates the Pareto front (Z_P), which consists of the objective vectors f(x) corresponding to each decision vector x in the Pareto set, as defined in Eq. (4) and illustrated in Fig. 1. Each member of the Pareto front is referred to as an alternative.

$$Z_P = \{\mathbf{f}(\mathbf{x}) | \mathbf{x} \in S_P\} \tag{4}$$

Based on the Pareto set and Pareto front, the SSSI decision-maker relies on the concepts of the Nadir point and the Utopia point. The Nadir point, denoted by ($\mathbf{z_{nd}}$) represents a vector in the (Z_P) space that captures the worst (maximum) values achieved by any objective vector in (Z_P) space as shown in Eq. (5). Conversely, the Utopia point, denoted by ($\mathbf{z}^*$), indicates the best (minimum) values attainable for each objective function in the (Z_P) space, as illustrated in Eq. (6).

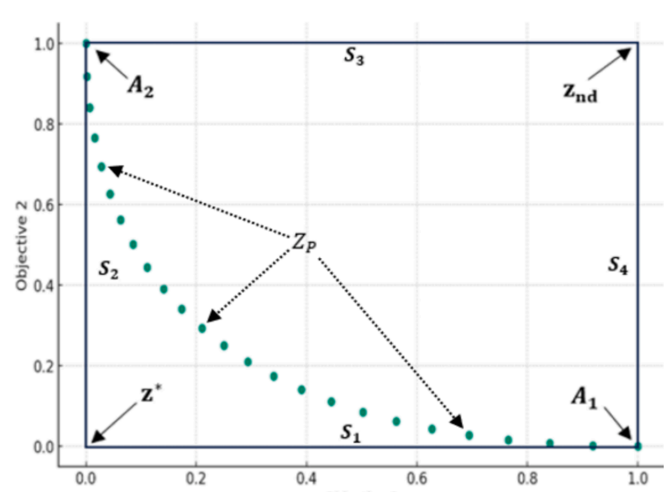

Fig. 1. Convex Pareto front points and the rectangular shape.

$$\mathbf{z_{nd}} = \left(\max_{f(\mathbf{x}) \in Z_P} f_1(\mathbf{x}), \cdots, \max_{f(\mathbf{x}) \in Z_P} f_k(\mathbf{x}) \right) \tag{5}$$

$$\mathbf{z}^* = \left(\min_{f(\mathbf{x}) \in Z_P} f_1(\mathbf{x}), \cdots, \min_{f(\mathbf{x}) \in Z_P} f_k(\mathbf{x}) \right) \tag{6}$$

However, in the SSSI decision making approach, the nadir and Utopia points are shown in Eq. (7) and Eq. (8) respectively.

$$\mathbf{z_{nd}} = \left(\max_{f(\mathbf{x}) \in Z_P} f_1(\mathbf{x}), \max_{f(\mathbf{x}) \in Z_P} f_2(\mathbf{x}) \right) \tag{7}$$

$$\mathbf{z}^* = \left(\min_{f(\mathbf{x}) \in Z_P} f_1(\mathbf{x}), \min_{f(\mathbf{x}) \in Z_P} f_2(\mathbf{x}) \right) \tag{8}$$

In addition to the Nadir and Utopia points, two other points, points ($\mathbf{A}_1$) and ($\mathbf{A}_2$), are introduced in Eq. (9) and Eq. (10), respectively, representing the two extremities of (Z_P).

$$\mathbf{A}_1 = \left(\min_{f(\mathbf{x}) \in Z_P} f_1(\mathbf{x}), \max_{f(\mathbf{x}) \in Z_P} f_2(\mathbf{x}) \right) \tag{9}$$

$$\mathbf{A}_2 = \left(\max_{f(\mathbf{x}) \in Z_P} f_1(\mathbf{x}), \min_{f(\mathbf{x}) \in Z_P} f_2(\mathbf{x}) \right) \tag{10}$$

These four points ($\mathbf{z_{nd}}$, $\mathbf{z}^*$, $\mathbf{A}_1$, and $\mathbf{A}_2$) create a rectangular shape has four sides ($\mathbf{S}_1$, $\mathbf{S}_2$, $\mathbf{S}_3$, and $\mathbf{S}_4$) as shown in Fig. 1.

However, to apply the SSSI method effectively, the rectangle must be transformed into a square by using a normalization technique. In this paper, the Max-Min approach is employed—a common method in multi-objective optimization for scaling objective function values to a uniform range. Eq. (11) presents the Max-Min normalization formula for all $f_k(\mathbf{x})$ values, where $\mathbf{x} \in S_P$ (Mazziotta & Pareto, 2022).

$$f_{k,\ norm}(\mathbf{x}) = \frac{f_k(\mathbf{x}) - \min_{f(\mathbf{x}) \in Z_P} f_k(\mathbf{x})}{\max_{f(\mathbf{x}) \in Z_P} f_k(\mathbf{x}) - \min_{f(\mathbf{x}) \in Z_P} f_k(\mathbf{x})} \tag{11}$$

In the resulting square shape, each side has the same length (a). The SSSI method considers a line connecting the Nadir and Utopia points—one of the two diagonals in this square, as illustrated in Fig. 2. This diagonal represents the slope (NU_{slop}) between the Nadir and Utopia points, as shown in Eq. (12).

$$NU_{slop} = \frac{\max_{f(\mathbf{x}) \in Z_P} f_1(\mathbf{x}) - \min_{f(\mathbf{x}) \in Z_P} f_1(\mathbf{x})}{\max_{f(\mathbf{x}) \in Z_P} f_2(\mathbf{x}) - \min_{f(\mathbf{x}) \in Z_P} f_2(\mathbf{x})} \tag{12}$$

Next, two perpendicular lines are drawn from point (P) on the diagonal (NU_{slop}). The first line meets side S1 at point (Q), and the second line meets side S2 at point (R). his construction creates two right-angled triangles, $\Delta PQ\mathbf{z}^*$ and $\Delta PR\mathbf{z}^*$, with right angles at points (Q) and (R), respectively, as shown in Fig. 2. Both triangles share the same hypotenuse $P\mathbf{z}^*$, which has length (d). The value of (d) can be computed for $\Delta PQ\mathbf{z}^*$ using Eq. (13) and for $\Delta PR\mathbf{z}^*$ using Eq. (14).

$$d = \sqrt{(PQ)^2 + (Q\mathbf{z}^*)^2} \tag{13}$$

$$d = \sqrt{(PR)^2 + (R\mathbf{z}^*)^2} \tag{14}$$

From Eq. (13) and Eq. (14)

$$\sqrt{(PQ)^2 + (Q\mathbf{z}^*)^2} = \sqrt{(PR)^2 + (R\mathbf{z}^*)^2} \tag{15}$$

Because the diagonal (NU_{slop}) bisects the right angle at $\mathbf{z}^*$ into two 45° angles, the triangles $\Delta PQ\mathbf{z}^*$ and $\Delta PR\mathbf{z}^*$ are isosceles right triangles, meaning their legs are equal in length. As a result, Eq. (15) can be rewritten as shown in Eq. (16).

$$\sqrt{(PQ)^2 + (PQ)^2} = \sqrt{(PR)^2 + (PR)^2} \tag{16}$$

From Eq. (16), it follows that the leg PQ in $\Delta PQ\mathbf{z}^*$ is equal to the leg PR in $\Delta PR\mathbf{z}^*$. Because these legs represent the distances from point P to sides S1 and S2 respectively—and are thus equal—point P on (NU_{slop}) is equidistant from both sides. Since sides S1 and S2 represent the scales of the first and second objective functions, respectively, any point on (NU_{slop}) maintains an equal distance from both objective functions. See (Fig. 3).

Based on the earlier proof, the SSSI method calculates two slopes for each alternative in the Pareto front. The first slope is between alternative (m) and the Nadir point, denoted as ($N_{(m)slop}$), and the second slope is between the same alternative and the Utopia point, denoted as ($U_{(m)slop}$) as shown in Fi. 3 and calculated in Eq. (17) and Eq. (18), respectively. The method then determines the average of these two slopes, $Avg_{(m)slop}$, as shown in Eq. (19).

$$N_{(m)slop} = \frac{f_{1(m)}(\mathbf{x}) - \min_{f(\mathbf{x}) \in Z_P} f_1(\mathbf{x})}{f_{2(m)}(\mathbf{x}) - \min_{f(\mathbf{x}) \in Z_P} f_2(\mathbf{x})} \tag{17}$$

$$U_{(m)slop} = \frac{\max_{f(\mathbf{x}) \in Z_P} f_1(\mathbf{x}) - f_{1(m)}(\mathbf{x})}{\max_{f(\mathbf{x}) \in Z_P} f_2(\mathbf{x}) - f_{2(m)}(\mathbf{x})} \tag{18}$$

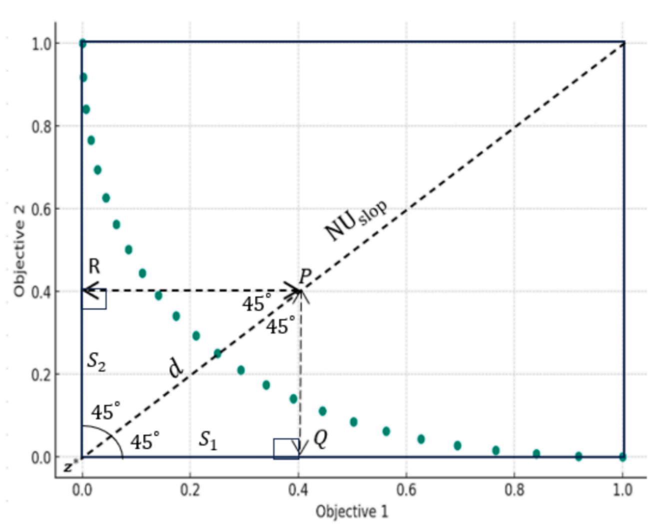

Fig. 2. The main slop (NU_{slop}).

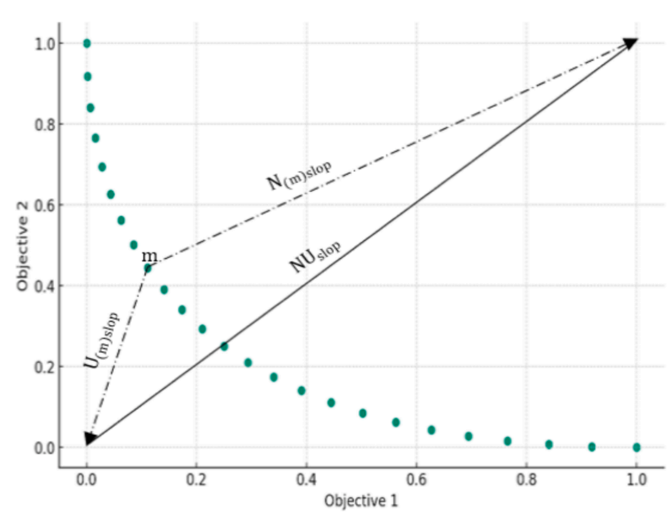

Fig. 3. SSSI slops.

$$\text{Avg}_{(m)slop} = \frac{N_{(m)slop} + U_{(m)slop}}{2} \tag{19}$$

Subsequently, the SSSI value for each alternative (m) is found by taking the absolute difference between ($\text{Avg}_{(m)slop}$) and (NU_{slop}) as given in Eq. (20).

$$\text{SSSI}_{(m)} = \left|\text{Avg}_{(m)slop} - NU_{slop}\right| \tag{20}$$

A lower SSSI value indicates that the alternative (m) is closer to (NU_{slop}), and hence closer to the region representing the most balanced trade-off between the two objective functions on the Pareto front. The SSSI method ranks all alternatives accordingly.

The SSSI decision-maker incorporates a criteria scale that allows controlling the priority ratio between two objective functions when ranking alternatives. This scale employs multiple Utopia and Nadir points to preserve the square shape used in SSSI calculations.

The priority scale for the first objective is (α), and for the second objective is (β), both ranging from 0 to 1. By default, $\alpha = \beta = 0$, which yields a solution reflecting an equally balanced trade-off between the two objectives on the Pareto front. Increasing one of these scales by a certain amount elevates the priority of its corresponding objective by the same percentage; after updating the Nadir and Utopia points accordingly, the square shape shifts to emphasize a specific region of the Pareto front.

Using the values of α and β along with the original Nadir and Utopia points defined in Eq. (7) and Eq. (8), the modified Nadir point ($\mathbf{z_{nd}}'$) and the modified Utopia point ($\mathbf{z}^{*'}$) are given in Eq. (21) and Eq. (22), respectively.

$$\mathbf{z_{nd}}' = (F_{1(N)}, F_{2(N)}) \tag{21}$$

$$\mathbf{z}^{*'} = (F_{1(U)}, F_{2(U)}) \tag{22}$$

Where $F_{1(N)}$, $F_{2(N)}$, $F_{1(U)}$, and $F_{2(U)}$ are calculated in equations (23) to (26).

$$F_{1(N)} = \max_{f(\mathbf{x})\in Z_P} f_1(\mathbf{x}) - \beta\left(\max_{f(\mathbf{x})\in Z_P} f_1(\mathbf{x}) - \min_{f(\mathbf{x})\in Z_P} f_1(\mathbf{x})\right) \tag{23}$$

$$F_{2(N)} = \max_{f(\mathbf{x})\in Z_P} f_2(\mathbf{x}) - \alpha\left(\max_{f(\mathbf{x})\in Z_P} f_2(\mathbf{x}) - \min_{f(\mathbf{x})\in Z_P} f_2(\mathbf{x})\right) \tag{24}$$

$$F_{1(U)} = \min_{f(\mathbf{x})\in Z_P} f_1(\mathbf{x}) + \alpha\left(\max_{f(\mathbf{x})\in Z_P} f_1(\mathbf{x}) - \min_{f(\mathbf{x})\in Z_P} f_1(\mathbf{x})\right) \tag{25}$$

$$F_{2(U)} = \min_{f(\mathbf{x})\in Z_P} f_2(\mathbf{x}) + \beta\left(\max_{f(\mathbf{x})\in Z_P} f_2(\mathbf{x}) - \min_{f(\mathbf{x})\in Z_P} f_2(\mathbf{x})\right) \tag{26}$$

These updated points subsequently generate new points ($\mathbf{A_1}$) and ($\mathbf{A_2}$) , as shown in Eq. (27) and Eq. (28), respectively.

$$\mathbf{A_1}' = (F_{1(U)}, F_{2(N)}) \tag{27}$$

$$\mathbf{A_2}' = (F_{1(N)}, F_{2(U)}) \tag{28}$$

However, when the priority scale for the first objective (α) is modified, $\mathbf{A_1}$ does not change, as illustrated by the dotted square in Fig. 4. Likewise, adjusting the priority scale for the second objective (β) leaves $\mathbf{A_2}$ unaffected, as shown by the dashed square. After defining the square shape based on the selected priority scale values, the SSSI method uses slope calculations to rank the alternatives within the resulting square.

The priority scale parameters α and β are independent from each other and range from 0 to 1. These parameters allow decision-makers to assign flexible and dynamic weights to each objective without being constrained by a fixed sum. This independence ensures that decision-makers can explore a wide range of trade-offs and customize their preferences without being limited by a predefined ratio between the objectives. Fig. 5 shows the flowchart of the proposed SSSI decision-making process.

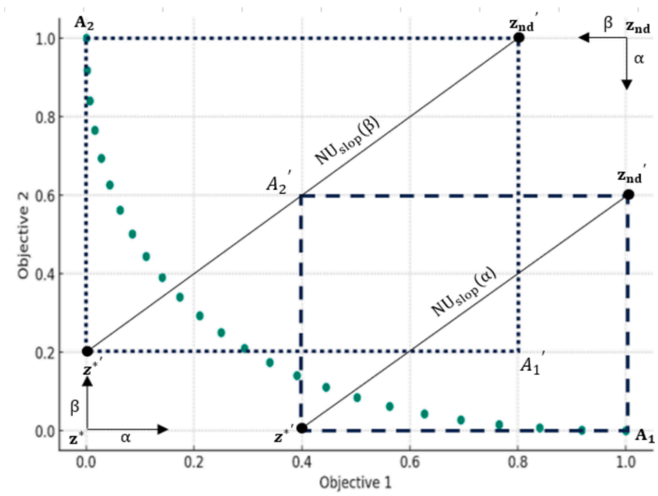

Fig. 4. The square shape and the main slope at different priority scale settings.

3. Methodology

The methodology in this paper aims to validate the performance of the SSSI method and assess its reliability for decision-making. To do so, the SSSI method is applied to various patterns and shapes of Pareto fronts from different bi-objective benchmarks. In addition, SSSI is compared with several other MCDM methods using two distinct comparison approaches to evaluate its effectiveness. The comparison also accounts for the stochastic nature of evolutionary algorithms by using NSGA-II for optimization and Pareto front generation.

3.1. Benchmarks

To evaluate the reliability of the SSSI method, it is tested on various 2D Pareto fronts to rank the alternatives. To accomplish this, different test functions from multiple benchmarks are optimized using the NSGA-II algorithm, producing diverse Pareto fronts. In this paper, the primary benchmark is ZDT, considered a standard for bi-objective optimization problems (Zitzler et al., 2000). ZDT allows the SSSI method to be examined on convex, non-convex, and discrete Pareto front shapes.

In addition to the ZDT benchmark, test functions from several others are employed to cover an array of Pareto front patterns. From the DTLZ benchmark, two test functions (DTLZ1 and DTLZ2) are used to explore linear and "discounted" Pareto front shapes (Deb et al., 2005). Because ZDT and DTLZ benchmarks are unconstrained, the CF benchmark from the Congress on Evolutionary Computation (CEC) is also included, as its functions are constrained (Zhang et al., 2009). Furthermore, the IMOP benchmark is incorporated to cover non-uniform Pareto fronts, where test functions generate non-uniformly distributed alternatives (Tian et al. 2019). The detailed characteristics of all benchmark datasets used in this study are provided in Appendix A.

3.2. The MCDM methods set

To assess the efficiency of the SSSI method, its performance is compared with a set of well-known Posteriori MCDM methods (Petrović et al., 2018). The first is VIKOR (Yu, 1973), which focuses on identifying a compromise solution based on proximity to an ideal solution, emphasizing trade-offs. The second is COPRAS (Zavadskas et al., 1994), which evaluates alternatives through normalized values and criteria weights to determine their relative effectiveness.

The third method in the comparison is TOPSIS (Trung, 2021), which locates the option closest to the ideal solution and farthest from the worst alternative based on geometric distances. Finally, GRA (Jana & Pal, 2021) measures alternatives by assessing the degree of similarity or

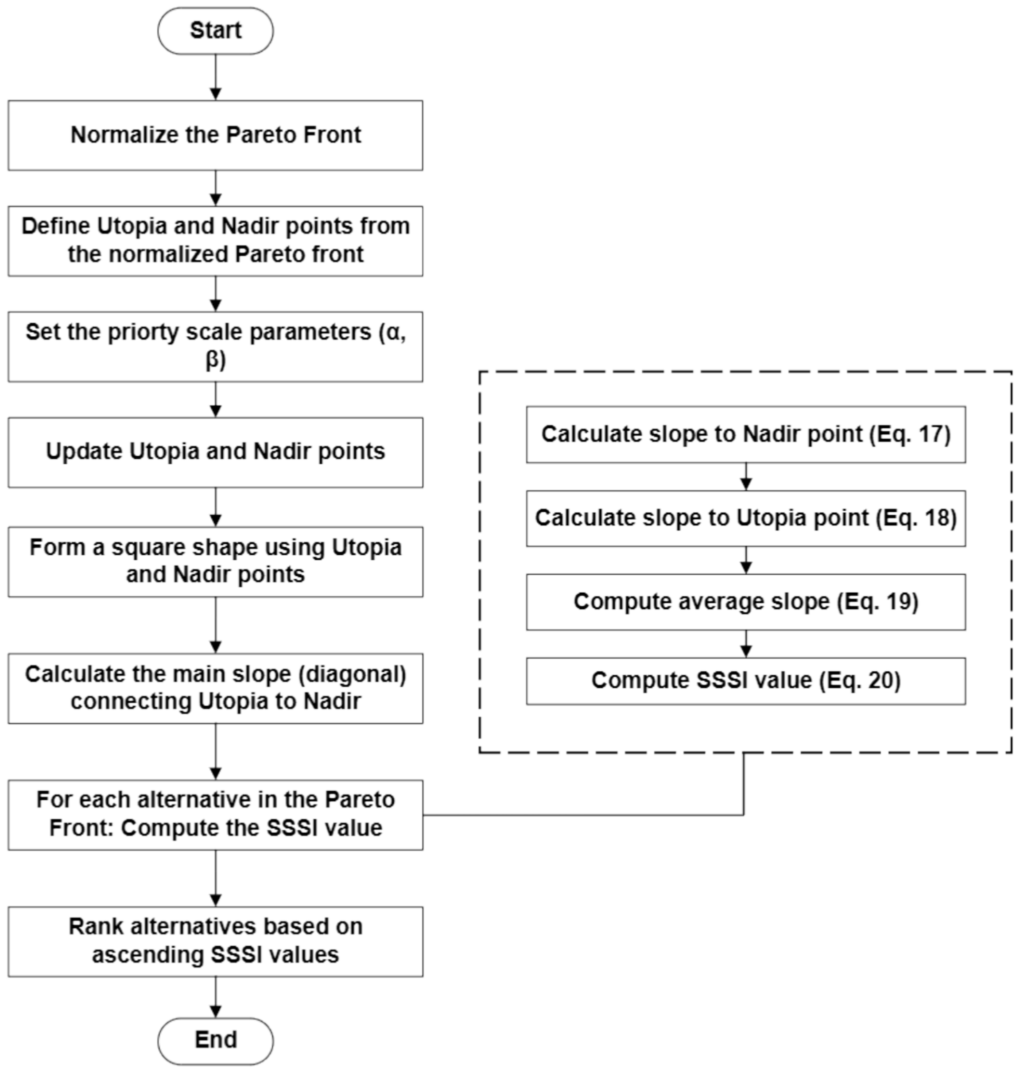

Fig. 5. Flowchart of the proposed SSSI decision-making process.

connection among different sequences.

These four methods were chosen for comparison with SSSI because they represent distinct and widely recognized approaches in multi-criteria decision-making, covering various perspectives—from compromise solutions and proximity-based assessments to proportional analyses and handling of uncertainty. Moreover, like SSSI, these methods are well-suited to the Min-Max normalization technique, ensuring a uniform basis for comparing diverse decision-making scenarios in bi-objective optimization. To ensure a fair and unbiased comparison, we intentionally used the basic forms of VIKOR, TOPSIS, COPRAS, and GRA, without incorporating advanced variations such as fuzzy logic or hybrid approaches. This decision allows for a transparent evaluation of the core methodologies and highlights the unique contributions of SSSI, such as its dynamic square framework and robustness in handling discontinuous Pareto fronts. These methods were chosen because they comprehensively represent key paradigms in decision-making, enabling a thorough and meaningful comparison.

3.3. Comparison analysis

The comparison between the SSSI method and the MCDM methods introduced in Section 3.2 is conducted using two approaches: a geometric approach and an analytical approach. The geometric approach visualizes the Pareto fronts from various benchmarks, highlighting the alternatives selected by each decision-maker and enabling a direct visual comparison. Meanwhile, the analytical approach utilizes two aggregation methods to compare the full ranking of alternatives generated by each decision-maker.

The first aggregation method in the analytical comparison is the Mean Absolute Deviation (MAD). This statistical measure quantifies the average absolute deviation of data points from their mean. In this paper, MAD assesses the consistency of the rankings produced by different decision-makers. When multiple decision-makers rank a set of alternatives, each ranking can be viewed as a data series. By calculating the MAD for each decision-maker's ranking, the degree of variability in their preferences can be evaluated. For a ranking with (n) alternatives, the mean value for alternative (io) is calculated using Eq. (25), while the absolute deviation for the same alternative is determined using Eq. (30). Finally, these absolute deviation values are used to compute the MAD value via Eq. (31) (Pham-Gia & Hung, 2001).

$$\text{Mean} = \frac{\sum_{io=1}^{n} At_{io}}{n} \tag{29}$$

$$\text{Absolute Deviation} = |At_{io} - \text{Mean}| \tag{30}$$

$$\text{MAD} = \frac{\sum_{io=1}^{n} |At_{io} - \text{Mean}|}{n} \tag{31}$$

Lower MAD values indicate that a decision-maker's rankings are more consistent or closer to their average ranking, implying a clearer preference pattern. By contrast, higher MAD values suggest greater variability and less definitive preferences. Comparing MAD values across decision-makers thus helps identify which ones exhibit more stable or consistent ranking patterns.

The second aggregation method in the analytical comparison approach is the Spearman's rank correlation coefficient, a non-parametric measure of the strength and direction of association between two ranked variables. A shown in Eq. (32), the Spearman's rank correlation coefficient was calculated using the sum of the squared differences between the ranks (Li et al., 2022). Where (rho) is the Spearman's rank correlation coefficient, (Σdf^2) is the squared differences between the ranks, and (rt) is the number of rank

$$\text{rho} = 1 - \frac{6 \times \Sigma df^2}{rt(rt^2 - 1)} \tag{32}$$

where (rho) is the Spearman's rank correlation coefficient, (Σdf^2) is the squared differences between the ranks, and (rt) is the number of ranks. This coefficient reflects how closely the rankings align: values near + 1 indicate a strong positive correlation, suggesting that the decision-makers generally agree on the rankings; values near –1 imply a strong negative correlation, indicating a fundamental disagreement; and values close to zero signify no correlation, pointing to independent or unrelated ranking preferences. In this paper, the Spearman's rank correlation coefficient will be used to evaluate how SSSI's performance compares to each of the MCDM methods listed in Section 3.2.

3.4. Real case scenarios

To validate the applicability of the proposed decision maker, two real-world scenarios were selected. These scenarios demonstrate the framework's ability to handle complex multi-objective optimization problems involving practical constraints and competing objectives. The first scenario focuses on energy distribution optimization, highlighting the trade-off between minimizing costs and reducing carbon emissions. The second scenario addresses investment portfolio optimization, where the objectives are to minimize risk and maximize returns.

3.4.1. Energy distribution optimization

The first real-world scenario addresses the optimization of energy distribution among six key sources: Solar, Wind, Nuclear, Fossil (Coal), Natural Gas, and Hydropower. In this scenario, the aim is to allocate energy generation from these sources to meet a total demand of 100 MWh, while minimizing the total energy cost ($) and the total carbon emissions (kg CO_2) (Lazard, 2021). Each energy source has unique characteristics, including cost per unit of energy produced, carbon emissions, and maximum capacity (International Energy Agency & Centre for Climate Finance & Investment, 2020). However, the total energy cost is calculated based on the per-unit cost of energy production for each source and the amount of energy allocated. These costs include factors such as fuel costs, operation and maintenance expenses, and capital recovery costs. This scenario is representative of real-world energy policy decisions, where affordability and sustainability often conflict.

In this optimization, the decision variables xm_i represent the energy allocated from each source, and the two objectives are minimizing the total energy cost $f_1(x)_E$, and the total carbon emissions $f_2(x)_E$ as shown in Eq. (33) and Eq. (34) respectively.

$$f_1(x)_E = \sum_{i=1}^{6} c_i \cdot xm_i \tag{33}$$

$$f_2(x)_E = \sum_{i=1}^{6} e_i \cdot xm_i \tag{34}$$

where c_i and e_i are the cost and emissions per MWh for source i. This optimization is subject to constraints that ensure that the total energy allocation equals the demand, remains non-negative, and does not exceed each source's maximum capacity.

The optimization of energy distribution often involves managing conflicting objectives under dynamic and uncertain conditions. Recent advancements in robust modeling and adaptive decision-making frameworks, such as those applied in battery lifecycle estimation and predictive maintenance, highlight the value of such methods (Wang et al., 2023). Inspired by these approaches, the SSSI framework facilitates effective trade-off analysis between minimizing energy costs and reducing emissions, enabling practical and adaptable solutions for real-world applications.

3.4.2. Investment portfolio optimization

This portfolio optimization scenario addresses the challenge of allocating a fixed budget across three well-known stocks—Amazon, Apple, and Tesla—using historical stock price data obtained from (Yahoo Finance, n.d.). The decision variables are the allocation weights, w_i, for each stock i, representing the proportion of the total budget invested in that stock. These weights must satisfy the constraints in Eq. (35) and Eq. (36) where the first ensures the entire budget is allocated, and the second limits overexposure to any single stock.

$$\sum_{i=1}^{3} w_i = 1 \tag{35}$$

$$0 \le w_i \le 0.5 \tag{36}$$

In this optimization, the two objectives are maximizing the total portfolio expected daily return by minimizing $f_1(x)_P$, and minimizing the total portfolio risk $f_2(x)_P$ measured using Conditional Value at Risk (CVaR), as shown in equations (37), (38), and (39) respectively (Chen & Zhou, 2022).

$$f_1(x)_P = \sum\nolimits_{i=1}^{3} - w_{id} \cdot r_{id} \tag{37}$$

$$f_2(x)_P = \sum\nolimits_{i=1}^{3} w_{id} \cdot \text{CVaR}_{id} \tag{38}$$

$$\text{CVaR}_\alpha = \frac{1}{N_\alpha} \sum_{id \in \{r_{id} \le \text{VaR}_\alpha\}} r_{id} \tag{39}$$

Where r_i is the expected return of stock i based on the historical price data, and CVaR_i is a measure of risk that quantifies the average loss in the worst-case scenarios beyond the confidence level (α) of stock (id), VaR is the return threshold below which a certain percentage of the worst losses occur, and N_α is the number of returns below the VaR threshold. In this study, the confidence level is 95 %, and VaR corresponds to the 5th percentile of the sorted daily returns (Chen & Zhou, 2022).

These objectives are inherently conflicting because stocks with higher expected returns, such as Tesla, often come with greater risks, as reflected by higher CVaR values in extreme market conditions. This conflict highlights the need for a robust decision-making approach to navigate the trade-offs between maximizing returns and minimizing risks. The optimization algorithm addresses this challenge by generating a Pareto front, which provides a range of optimal solutions representing different risk-return balances. The proposed decision maker plays a crucial role in this scenario by selecting the most suitable solution from the Pareto front, effectively tailoring the portfolio to align with specific risk tolerance and return expectations. This demonstrates the decision maker's importance in achieving well-informed, balanced investment strategies in complex financial environments.

3.5. Evolutionary algorithm

In this paper, the stochastic nature of evolutionary algorithms is incorporated into the comparison analysis. To this end, the NSGA-II (Non-dominated Sorting Genetic Algorithm II) was chosen to generate Pareto fronts for evaluation by the SSSI method and the MCDM methods introduced in Section 3.2.

NSGA-II is a widely adopted evolutionary algorithm for multi-objective optimization. It simulates natural selection by iteratively evolving a population of solutions through selection, crossover, and mutation. Three core features enable NSGA-II to achieve its objectives: (1) Fast Non-Dominated Sorting, which categorizes solutions into Pareto fronts based on dominance; (2) Crowding Distance, preserving diversity by favoring solutions in less crowded regions; and (3) Elitism, which maintains the best solutions across generations by merging parent and offspring populations (Deb et al., 2002). These characteristics make NSGA-II ideal for producing diverse, well-distributed Pareto fronts, as required in this study.

Here, the mutation rate, mutation strength, and crossover rate for NSGA-II were fixed at 0.05, 0.5, and 0.9, respectively, while population size and the number of generations varied depending on the test function and the specific comparison analysis. However, because NSGA-II is inherently stochastic, each run may yield a different Pareto front due to random initialization and genetic operations. To account for this variability, NSGA-II was executed 100 times for each test function. At each run, the comparison method was applied, and the mean values across the 100 iterations were used to ensure robust, reliable comparisons between the SSSI method and the other MCDM approaches.

4. Results and discussion

4.1. Benchmarks

Using NSGA-II to minimize the bi-objective function ZDT1 from the ZDT benchmark yields a set of optimal, non-dominated solutions—each referred to as an alternative (At). These alternatives form a convex Pareto front, as illustrated in Fig. 6.

From the Pareto front in Fig. 5, the decision matrix for the ZDT1 function is presented in Table 1, along with the ranking of alternatives based on their SSSI values at the default priority scale.

The results indicate that alternatives 4, 5, 6, 7, and 8, representing the “knee” region of the analyzed Pareto front, have lower SSSI values compared to the other alternatives. Notably, alternative 5 exhibits the lowest SSSI value, making it the optimal solution to minimize the ZDT1

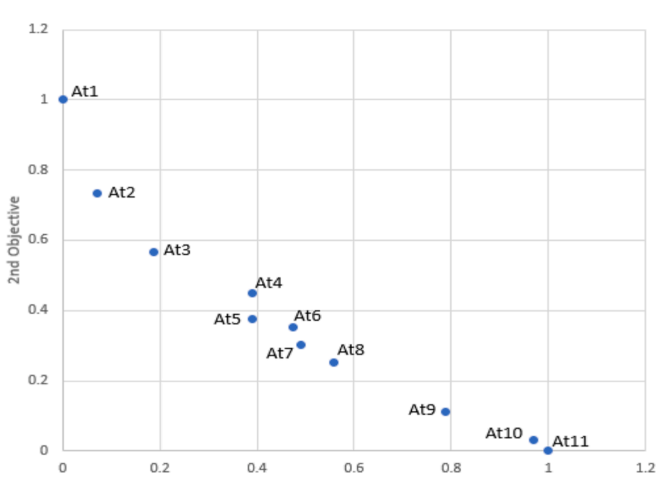

Fig. 6. Pareto front of the Non-Dominate Solutions for Optimizing ZDT1 Function using NSGA-II.

Table 1
Decision Matrix and SSSI Ranking for the ZDT1 Pareto front.

Decision Matrix			SSSI Ranking (α = 0, β = 0)	
Alternative	1st Objective	2nd objective	Alternative Rank	SSSI Value
At1	0	1	11	INFINITY
At2	0.0712	0.7331	8	5.0045
At3	0.1869	0.5677	6	1.2529
At4	0.3893	0.4485	2	0.1245
At5	0.39	0.3755	1	0.030475
At6	0.473	0.3526	3	0.2415
At7	0.4891	0.3007	4	0.37698
At8	0.559	0.2523	5	0.62206
At9	0.7877	0.1125	7	2.0188
At10	0.9681	0.0313	9	15.167
At11	1	0	11	INFINITY

bi-objective function under an equally balanced trade-off between the two objectives, both of which have equal priority. Additionally, the two least-favored alternatives in the SSSI ranking share the same SSSI value, which is infinite. These alternatives correspond to points $\mathbf{A}_1$ and $\mathbf{A}_2$, which—together with the Nadir and Utopia points—form the SSSI rectangle.

However, Table 2 presents the optimal alternative selected by the SSSI method under various priority scale settings. The first two settings adjust the priority scale for the first objective (α) to 0.2 and 0.7, respectively, while the last two settings modify the priority scale for the second objective (β) to 0.35 and 0.9, respectively.

From Table 2, it is evident that the SSSI value of the optimal alternative at each scale setting differs from its SSSI value at the default settings shown in Table 1. Meanwhile, Table 3 provides the complete alternative rankings from different decision-makers, allowing a direct comparison with the SSSI ranking when all methods are applied to the same decision matrix in Table 1.

Table 3 reveals that each decision-maker produces a distinct ranking for the same set of alternatives. Comparing these rankings with the SSSI ranking shows that VIKOR is the only method matching SSSI’s rank for alternative 5, while TOPSIS is the only method aligning with SSSI’s rank for alternative 3. Furthermore, the positions of alternatives 1, 10, and 11 remain the same across all rankings. To evaluate these rankings analytically, Table 4 presents the Spearman’s rank correlation coefficient values, indicating how closely each method’s ranking aligns with SSSI.

Notably, VIKOR has the rho value closest to 1, making it the most similar to SSSI, whereas COPRAS shows the least similarity. While Table 4 provides a method-by-method comparison with SSSI, Table 5 reports the Mean Absolute Deviation (MAD) values for all rankings together, offering an overall view of their consistency and variability.

Since lower MAD values indicate that a decision-maker’s ranking is more consistent or closer to its average ranking, Table 5 shows that SSSI and VIKOR are the most consistent in this comparison, followed by TOPSIS, then GRA, and finally COPRAS, which proves to be the least consistent of all the rankings.

It is important to note that the decision matrix in Table 1 and the alternative rankings in Table 3 correspond to the deterministic Pareto front generated by NSGA-II in Fig. 6. However, due to the stochastic nature of evolutionary algorithms such as NSGA-II, subsequent runs may produce different Pareto fronts even with the same test function and identical algorithm settings. Fig. 7 illustrates how the number of

Table 2
Optimal alternative chosen by SSSI at different priority scale settings.

Setting Number	Priority Scale	Optimal Alternative	SSSI Value
1	α = 0.2 β = 0	At7	0.031415
2	α = 0.7 β = 0	At9	0.1998
3	α = 0 β = 0.35	At4	0.4817
4	α = 0 β = 0.6	At2	0.52882

Table 3
Complete ranking of ZDT1 decision matrix alternatives from different decision makers.

Alternative Number (At)	Rankings				
	SSSI	VIKOR	TOPSIS	COPRAS	GRA
At1	11	11	11	11	11
At2	8	7	8	4	7
At3	6	2	6	1	3
At4	2	5	1	7	2
At5	1	1	3	2	5
At6	3	4	2	6	4
At7	4	3	4	3	1
At8	5	6	5	5	6
At9	7	8	7	8	8
At10	9	9	9	9	9
At11	11	11	11	11	11

Table 4
Spearman's rank correlation coefficients values between SSSI ranking and other rankings for ZDT1 decision matrix alternatives.

Decision Maker	rho
VIKOR	0.8455
TOPSIS	0.8273
COPRAS	0.3364
GRA	0.5909

Table 5
Mean Absolute Deviation (MAD) values for decision maker rankings (ZDT1).

Decision Maker	MAD
SSSI	1.05
VIKOR	1.05
TOPSIS	1.3
COPRAS	1.78
GRA	1.49

alternatives varies across 100 runs of NSGA-II when optimizing the ZDT1 test function under fixed conditions.

Fig. 7 shows that the number of alternatives varies between 5 and 13 across different iterations, with changes in both the values and locations of the alternatives on the Pareto front. This variability results in a different decision matrix for each iteration, leading to different rankings of alternatives. Consequently, this variation impacts the MAD and rho values in the comparison analysis. Fig. 8 illustrates the variations in the MAD value for SSSI over 100 iterations, as it is compared with the rankings of other decision-makers at each iteration.

As shown in Fig. 8, the MAD value for the SSSI method fluctuates between 0 and 2. A MAD value of 0 for SSSI at a specific iteration indicates that all decision-makers produced identical rankings during that iteration, resulting in zero MAD values for all methods. This situation is more likely to occur when the number of alternatives is lower, as smaller sets of alternatives increase the likelihood of identical rankings, as evidenced in Figs. 7 and 8.

Fig. 9 illustrates the rho values between the SSSI rankings and the rankings from other decision-makers over 100 iterations, highlighting the variability caused by changes in the Pareto front. The results indicate that TOPSIS rankings are the closest to SSSI rankings, with the majority of rho values near + 1, followed by GRA rankings, then VIKOR rankings. Conversely, COPRAS rankings are the least similar to SSSI rankings, as they exhibit the lowest number of rho values close to + 1. It is also notable that, while Table 4 shows VIKOR rankings as the closest to SSSI rankings for a deterministic Pareto front, this may not hold true when accounting for multiple runs of the algorithm under identical settings. To address the stochastic nature of NSGA-II, Table 6 presents the mean values of MAD and rho for each decision-maker across the 100 iterations.

According to the rho values in Table 6, the TOPSIS ranking is the closest to the SSSI ranking over 100 iterations of optimizing the ZDT1 test function, followed by GRA and VIKOR rankings. COPRAS rankings show the lowest similarity with SSSI rankings. Additionally, the SSSI ranking has the lowest average MAD value (0.773), indicating that it provides the most consistent rankings, remaining closer to the average ranking across the 100 iterations.

The results in Tables 5 and 6 also demonstrate that a decision-maker with a better MAD value at a single iteration does not necessarily maintain this advantage when considering the average MAD value over multiple iterations. The same applies to rho values, as seen when comparing Tables 4 and 6. Furthermore, the comparison in Table 6 has been expanded in Table 7, which presents the average MAD and rho values for each decision-maker across 100 iterations of optimizing several test functions from four benchmarks (ZDT, DTLZ, CF, and IMOP) using NSGA-II.

The results in Table 7 highlight SSSI's exemplary performance in the ZDT benchmark functions, particularly ZDT1, ZDT2, and ZDT3, where it achieved the lowest MAD values, demonstrating superior consistency in ranking solutions. This stands in contrast to other decision-makers, such as VIKOR and TOPSIS, which, while competitive, did not consistently achieve comparably low MAD values in these tests.

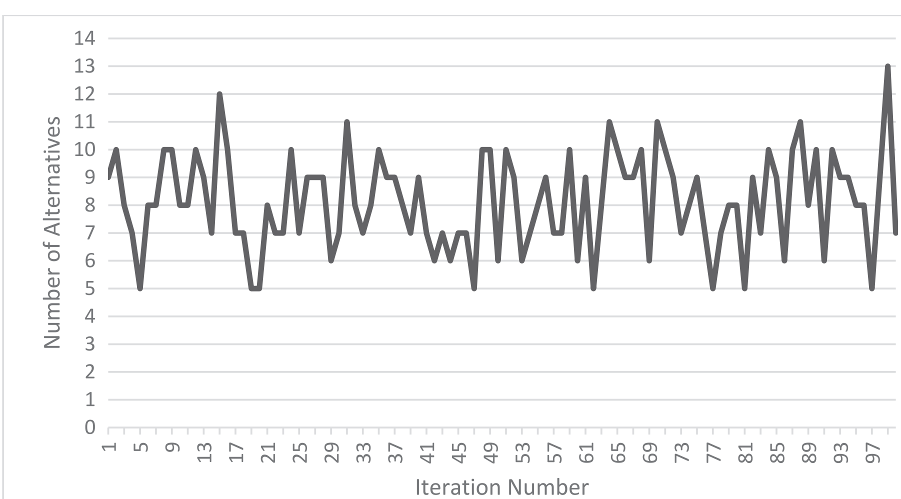

Fig. 7. Variation in the Number of Pareto Front Alternatives Over 100 Iterations (ZDT1).

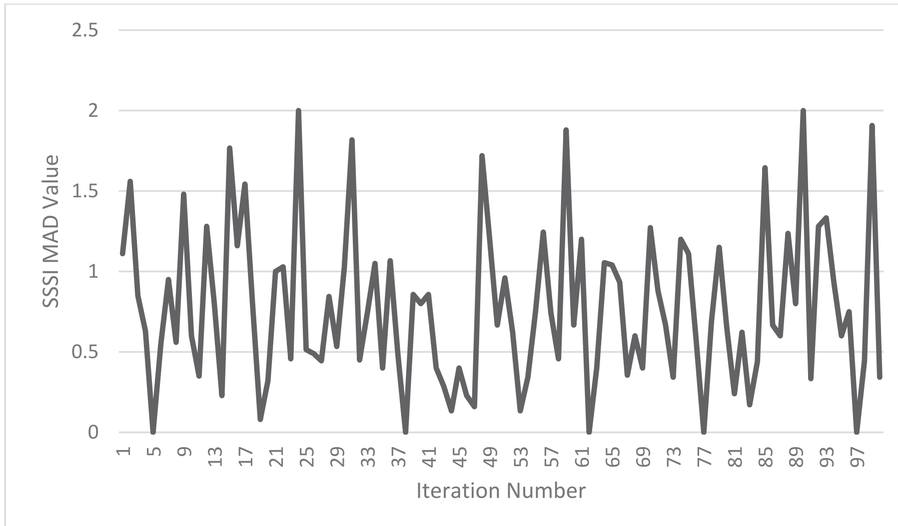

Fig. 8. Variation of MAD Value for SSSI Over 100 Iterations (ZDT1).

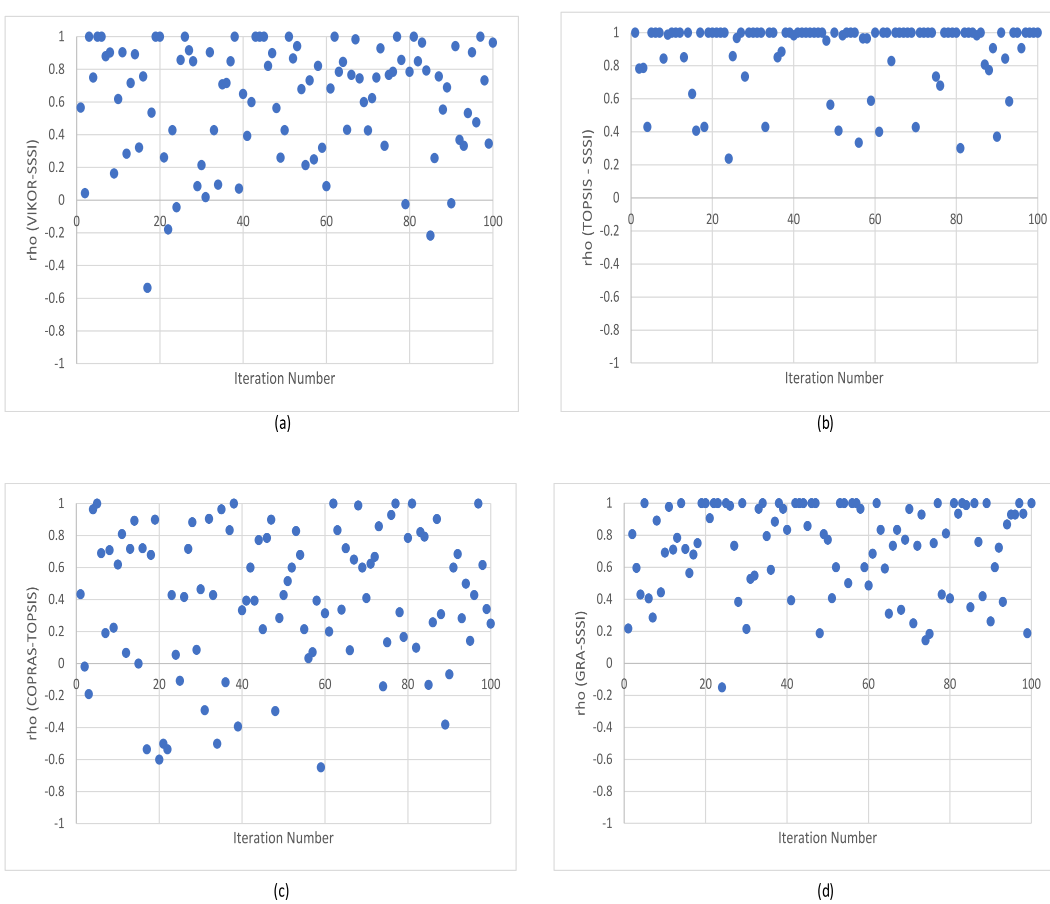

Fig. 9. Spearman's Rank Correlation Coefficients Between SSSI Rankings and Other Methods for ZDT1 Decision Matrix Alternatives Over 100 Iterations: (a) VIKOR, (b) TOPSIS, (c) COPRAS, and (d) GRA.

Table 6
Average MAD and rho values for each decision maker over the 100 iterations of optimizing ZDT1 function using NSGA-II.

Decision Maker	MAD	rho
SSSI	0.773	–
VIKOR	0.907	0.62
TOPSIS	0.825	0.884
COPRAS	1.153	0.41
GRA	0.893	0.75

In the IMOP benchmark, specifically IMOP1 and IMOP2, SSSI excelled again, showcasing its capability in handling non-uniform convex and non-convex Pareto fronts. However, its performance in the CF benchmark was more mixed; while SSSI performed strongly in some cases, it was outperformed by decision-makers like COPRAS and VIKOR in the CF6 function, indicating variability in constrained environments. In the DTLZ benchmarks, SSSI demonstrated further strength, particularly in DTLZ1, where its performance was on par with or exceeded that of other decision-makers.

For Spearman's rho values, SSSI's ranking approach demonstrated the highest correlation with TOPSIS in the ZDT benchmark, indicating a similar evaluation of solutions in these scenarios. In the IMOP benchmarks, SSSI's rankings exhibited a strong correlation with models like GRA, reflecting a shared prioritization strategy for managing complex Pareto front shapes. In contrast, the CF benchmark showed varying levels of correlation, with no single decision-maker consistently aligning with SSSI's rankings, highlighting the unique nature of SSSI's approach in constrained scenarios. The DTLZ benchmarks also revealed varying degrees of correlation, further emphasizing the distinctiveness of SSSI's decision-making methodology.

Overall, when comparing decision-makers based on the frequency of achieving the lowest MAD values, SSSI emerges as the most consistent performer, achieving the lowest MAD values in 12 out of the 15 test functions. This significant achievement underscores SSSI's robustness and reliability across a wide range of multi-objective optimization scenarios. Its consistency in performance surpasses that of other decision-makers, establishing SSSI as a particularly strong model in situations where stable and reliable rankings are essential.

To compare the performance of SSSI with other decision-makers geometrically, Fig. 10 illustrates the optimal alternatives selected by SSSI, VIKOR, TOPSIS, COPRAS, and GRA when applied to Pareto fronts generated by NSGA-II while optimizing four test functions: ZDT1, ZDT2, IMOP1, and IMOP2.

Fig. 10 depicts two convex Pareto fronts (ZDT1 and IMOP1) and two non-convex Pareto fronts (ZDT2 and IMOP2). While the points on the ZDT1 and ZDT2 Pareto fronts are uniformly distributed, those on the IMOP1 and IMOP2 Pareto fronts are non-uniformly distributed. From Fig. 10, it is evident that SSSI demonstrates consistent performance across both uniform and non-uniform Pareto fronts, highlighting its robust decision-making methodology, which relies on the scale of the Pareto front itself. This contrasts with other decision-making models, such as GRA, which may be influenced by the distribution of points on the Pareto front. Notably, VIKOR closely mirrors SSSI's performance, demonstrating a similar level of proficiency and adaptability, followed by TOPSIS as the next closest in performance. Fig. 11 provides another geometric analysis of the decision-makers' performance on test functions that generate more complex and discontinuous Pareto fronts.

The discontinuity in the ZDT3 and DTLZ7 Pareto fronts has minimal impact on the performance of SSSI and other decision-makers, as their results remain close to one another. This is primarily because most of the knee region does not lie within the discontinuous portions of the Pareto front, as shown in Fig. 11(a) for the ZDT3 function, and to a slightly lesser extent for DTLZ7 in Fig. 11(b). Conversely, for the IMOP3 and CF2 Pareto fronts in Fig. 11(c) and 11(d), respectively, decision-making becomes more challenging as the knee region is more prominently located within the discontinuous parts of the Pareto front. This results in greater variability among the outcomes of the decision-makers.

The SSSI framework was evaluated on a diverse set of Pareto front shapes, including convex, non-convex, and discontinuous fronts,

Table 7
Average MAD and rho values for each decision maker over 100 iterations across different test functions.

Benchmark	Function	Aggregation Method	Decision Maker				
			SSSI	VIKOR	TOPSIS	COPRAS	GRA
ZDT	ZDT1	MAD	0.66	0.77	0.67	1	0.76
		rho	–	0.61	0.88	0.4	0.78
	ZDT2	MAD	0.41	0.44	0.49	0.69	0.64
		rho	–	0.91	0.89	0.66	0.73
	ZDT3	MAD	0.83	1.29	0.91	1.54	1.84
		rho	–	0.23	0.85	−0.011	0.85
	ZDT4	MAD	0.39	0.37	0.36	0.51	0.44
		rho	–	0.78	0.97	0.67	0.77
	ZDT6	MAD	0.31	0.31	0.35	0.56	0.42
		rho	–	0.91	0.89	0.69	0.86
DTLZ	DTLZ1	MAD	0.65	0.94	0.75	1.4	0.67
		rho	–	0.45	0.84	−0.1	0.92
	DTLZ7	MAD	0.31	0.35	0.34	0.51	0.35
		rho	–	0.75	0.88	0.52	0.89
CF	CF1	MAD	0.51	0.55	0.77	0.68	0.6
		rho	–	0.75	0.59	0.6	0.77
	CF2	MAD	1.27	1.29	1.95	1.46	1.35
		rho	–	0.48	0.13	0.28	0.55
	CF3	MAD	1.09	1.11	1.72	1.23	1.17
		rho	–	0.46	0.14	0.3	0.6
	CF5	MAD	1	1.73	1	2	1.02
		rho	–	0.1	0.96	−0.1	0.9
	CF6	MAD	1.1	1	1.1	0.99	1.13
		rho	–	0.55	0.4	0.41	0.58
IMOP	IMOP1	MAD	0.91	0.8	1.3	0.8	1.02
		rho	–	0.77	0.4	0.7	0.67
	IMOP2	MAD	0.6	0.6	0.8	0.78	0.98
		rho	–	0.9	0.76	0.75	0.63
	IMOP3	MAD	0.95	1.3	0.96	1.6	0.98
		rho		0.25	0.77	−0.017	0.78

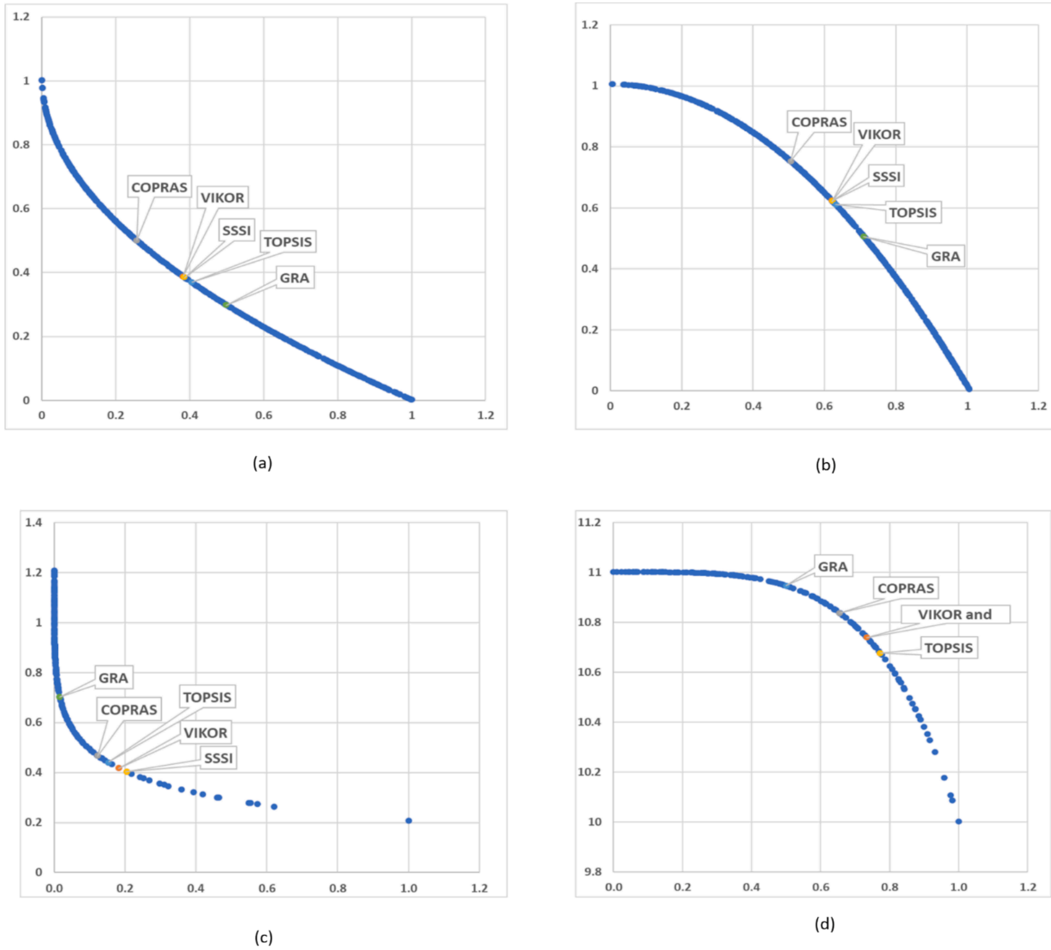

Fig. 10. Decision maker choices for the optimal alternative on different Pareto fronts from various test functions ((a) ZDT1, (b) ZDT2, (c) IMOP1, (d) IMOP2).

demonstrating its adaptability in multi-objective optimization. For example, in the ZDT1 benchmark (convex front), SSSI effectively identified knee region solutions. On non-convex fronts such as those in the IMOP and DTLZ benchmarks, it maintained consistent rankings, while on discontinuous fronts like ZDT3 and CF2, it exhibited robust performance despite the fragmented regions. These results underscore SSSI's flexibility and reliability across varied optimization scenarios.

4.2. Case studies

Fig. 12 shows the Pareto front generated from the energy distribution optimization scenario, demonstrating the trade-offs between minimizing total energy cost ($) and total carbon emissions (kg CO_2). Each point on the Pareto front represents a potential energy allocation strategy, highlighting the inherent complexity of balancing economic efficiency with environmental sustainability.

To evaluate the effectiveness of the proposed decision maker, SSSI, the Pareto front was analyzed under different Priority Scale settings. Table 8 summarizes the results of applying SSSI to the Pareto front under seven distinct Priority Scale settings where each setting adjusts the relative priority given to the two objectives.

When equal priority is given to both objectives as shown in setting 1, SSSI selects a balanced solution with moderate cost ($2907.7) and emissions (2969.4 kg CO_2). As the priority for cost increases in setting 4, the total cost drops significantly to $528.8, but this comes at the expense of drastically higher emissions (5169.9 kg CO_2). Conversely, when the focus shifts to reducing emissions (setting 7), emissions are minimized to 729.57 kg CO_2, but the cost rises substantially to $4988. The chart in Fig. 13 provides a visual representation of the energy allocations across the six sources for each Priority Scale setting. The stacked bar chart highlights how the SSSI decision maker adjusts the energy mix based on the relative importance of minimizing cost or emissions.

The second case study involves investment portfolio optimization, where the goal is to balance two competing objectives: minimizing total portfolio risk, measured as Conditional Value at Risk (CVaR), and maximizing the expected daily return. The Pareto front, shown in Fig. 14, consists of 188 solutions, each representing a trade-off between these two objectives.

The SSSI decision maker is applied to the normalized version of the Pareto front in Fig. 14 to validate its capability in identifying optimal portfolios that align with varying risk and return priorities. Table 9 summarizes the results of applying SSSI to the Pareto front under seven distinct Priority Scale settings where each setting adjusts the relative priority given to the two objectives.

Notably, the sensitivity of the SSSI Priority Scale is evident in Setting 2, where even a slight adjustment in the priority scale results in a noticeable shift in the selected optimal portfolio. This indicates the responsiveness of the decision maker to fine-tuned preference changes. In settings prioritizing expected return, the portfolio achieves a higher return (0.608 %) but with greater associated risk (CVaR = 1.6947) as shown in Setting 4. Conversely, in settings prioritizing risk reduction, the portfolio achieves the lowest risk (CVaR = 1.2053) but at the expense of lower expected returns 0.335 % as shown in Setting 7. The chart in Fig. 15 provides a visual representation of the budget allocation for the three assets (Amazon, Apple, and Tesla) under the seven SSSI Priority Scale settings.

The chart highlights how the allocation adjusts based on the relative priorities assigned to minimizing risk (CVaR) or maximizing expected

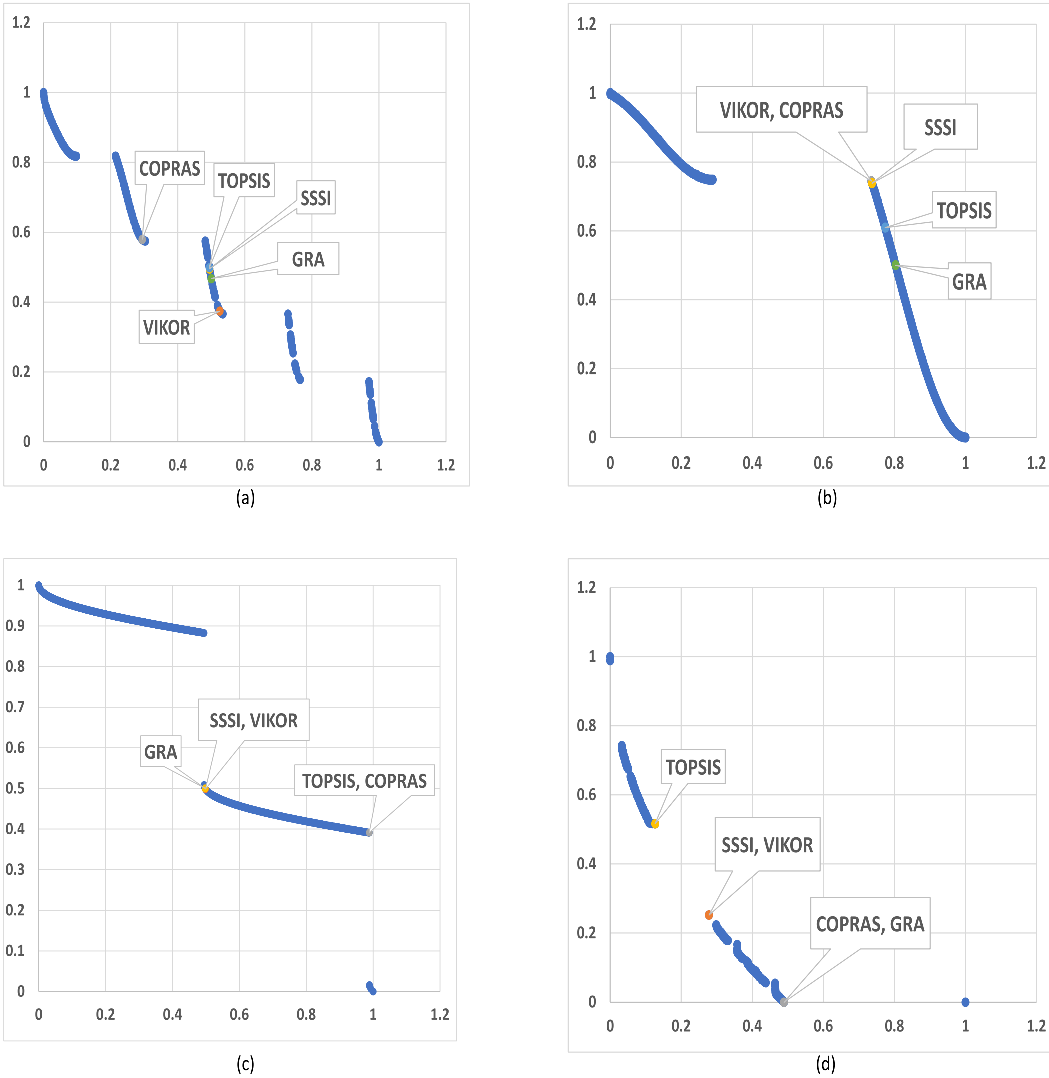

Fig. 11. Decision maker choices for the optimal alternative on different Pareto fronts from different test functions ((a) ZDT3, (b) DTLZ7, (c) IMOP3, (d) CF2).

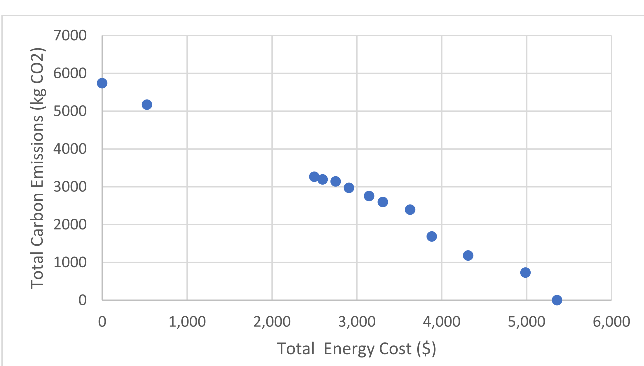

Fig. 12. Pareto Front Representing Energy Cost and Carbon Emissions Trade-offs.

return. For example, in Setting 7, which emphasizes minimizing risk, Amazon receives a substantial portion of the budget due to its lower volatility. Conversely, in settings prioritizing expected return, such as Setting 4, Tesla gains a larger share of the allocation due to its higher return potential. Apple, on the other hand, maintains a relatively stable allocation across all settings, suggesting that its return-risk profile is well-balanced and consistently valuable regardless of the priority scale.

Table 8
Energy Allocation Across Different SSSI Priority Scale Settings.

Setting Number	SSSI Priority Scale		Optimal Alternative	
	1st Objective Priority (α)	2nd Objective Priority (β)	1st Objective: Total Energy Cost ($)	2nd Objective: Total Carbon Emissions (kg CO2)
1	0	0	2907.7	2969.4
2	0.01	0	2751	3138.3
3	0.08	0	2597.4	3192.1
4	0.6	0	528.8	5169.9
5	0	0.07	3145.2	2751.6
6	0	0.15	3307.2	2593.3
7	0	0.8	4988	729.57

These results demonstrate the SSSI framework's adaptability in identifying optimal solutions that align with varying priorities, offering decision-makers the flexibility to address specific goals. This capability is essential for balancing competing objectives, such as affordability and sustainability in energy systems or risk and return in financial portfolios, making the SSSI framework a valuable tool for real-world applications in diverse and dynamic decision-making environments.

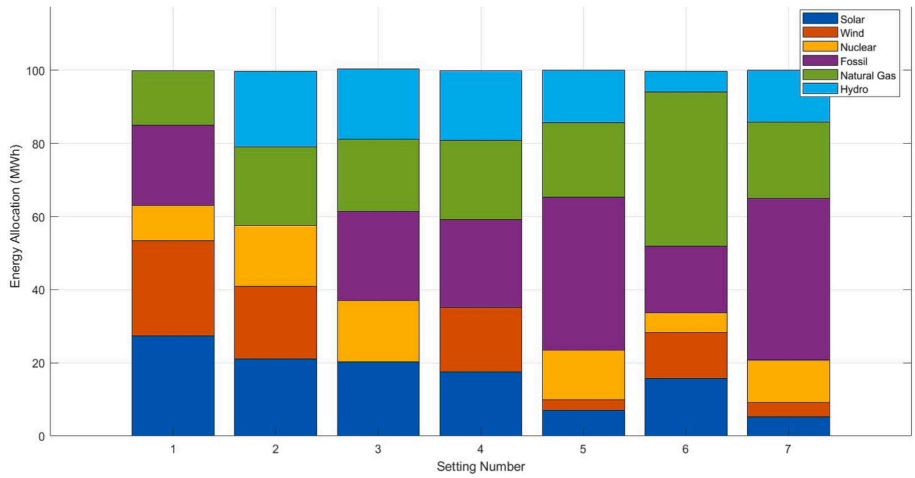

Fig. 13. Energy Allocations (MWh) Across Sources for Each Priority Scale Setting.

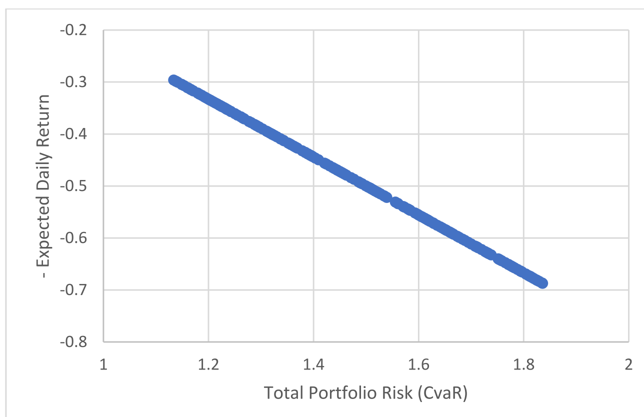

Fig. 14. Pareto Front Representing (CVaR) and (− Expected Daily Return) Trade-offs.

Table 9
Portfolio Allocation Across Different SSSI Priority Scale Settings.

Setting Number	SSSI Priority Scale		Optimal Alternative		
	1st Objective Priority (α)	2nd Objective Priority (β)	1st Objective		2nd Objective: Total Portfolio Risk (CVaR)
			$f_1(x)_P$ Value	Total Portfolio Expected Daily Return (I $f_1(x)_P$ I%)	
1	0	0	−0.492	0. 492 %	1.4857
2	0.007	0	−0.494	0. 494 %	1.4892
3	0.2	0	−0.5312	0. 531 %	1.5561
4	0.6	0	−0.608	0. 608 %	1.6947
5	0	0.01	−0.481	0.481 %	1.4664
6	0	0.4	−0.413	0.413 %	1.3441
7	0	0.8	−0.335	0.335 %	1.2053

5. Conclusion

This paper introduced the Square Shape Slope Index (SSSI) as a novel multi-criteria decision-making method for bi-objective optimization Pareto fronts. The conceptual framework and operational methodology of SSSI, grounded in the use of multiple Utopia and Nadir points governed by a priority scale, were detailed to emphasize its unique and straightforward approach, which leverages the geometric properties of the Pareto front.

The performance of SSSI was compared against other decision-making methods across a range of Pareto front shapes and patterns, including convex, non-convex, uniform, non-uniform, and discontinuous fronts. These fronts were generated by optimizing constrained and non-constrained test functions using NSGA-II. The results validated SSSI's reliability and effectiveness across diverse Pareto front configurations. Analytical comparisons using the MAD approach highlighted SSSI's superiority in decision-making, while geometric comparisons demonstrated its consistent performance, further reinforcing its reliability.

In conclusion, the findings presented in this paper confirm the uniqueness and effectiveness of SSSI, establishing it as a robust and reliable tool for bi-objective optimization problems. Future work will

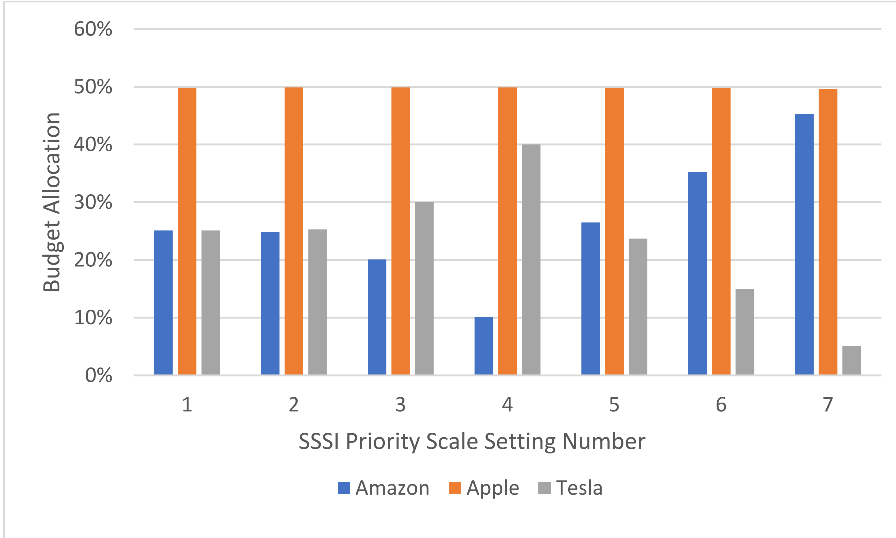

Fig. 15. Budget Allocations for Each Priority Scale Setting.

focus on extending the SSSI framework and methodology to accommodate multi-objective optimization involving more than two objectives.

CRediT authorship contribution statement

Bilal H. Al-Majali: Conceptualization, Investigation, Methodology, Formal analysis, Software, Writing – original draft, Visualization. **Ahmed F. Zobaa:** Supervision, Writing – review & editing, Project administration.

Declaration of competing interest

The authors declare that they have no known competing financial interests or personal relationships that could have appeared to influence the work reported in this paper.

Appendix A

Table A1
Characteristics of ZDT, DTLZ, CF, and IMOP benchmarks.

Benchmark	Test Function	Objectives (f_1 and f_2)	Constraints and Boundaries
IMOP	IMOP 1	$f_1(\mathbf{x}) = g(\mathbf{x}) + \cos\left(y_1\frac{\pi}{2}\right)^8 f_2(\mathbf{x}) = g(\mathbf{x}) + \sin\left(y_1\frac{\pi}{2}\right)^8 y_1 = \left(\frac{1}{5}\sum_{i=1}^{5} x_i\right)^{a_1} g(\mathbf{x}) = \sum_{i=K+1}^{10}(x_i - 0.5)^2, \overline{x}_{1:5}$	$0 \le x_i \le 1$
	IMOP 2	$f_1(\mathbf{x}) = g(\mathbf{x}) + \sqrt{\cos(y_1\pi/2)} f_2(\mathbf{x}) = g(\mathbf{x}) + \sqrt{\sin(y_1\pi/2)} y_1 = \left(\frac{1}{5}\sum_{i=1}^{5} x_i\right)^{0.05} g(\mathbf{x}) = \sum_{i=5+1}^{10}(x_i - 0.5)^2$	$0 \le x_i \le 1$
	IMOP3	$f_1(\mathbf{x}) = \sum_{i=5+1}^{10}(x_i - 0.5)^2 + \left[1 + \frac{\cos(10\pi y_1)}{5} - y_1\right] f_2(\mathbf{x}) = \sum_{i=5+1}^{10}(x_i - 0.5)^2 + y_1 y_1 = \left(\frac{1}{5}\sum_{j=1}^{5} x_j\right)^{0.05}$	$0 \le x_i \le 1$
CF	CF1	$f_1(\mathbf{x}) = x_1 + 2\cdot\frac{1}{\vert J_1\vert}\sum_{j\in J_1}\left(x_j - x_1^{p_j}\right)^2 f_2(\mathbf{x}) = (1 - x_1) + 2\cdot\frac{1}{\vert J_2\vert}\sum_{j\in J_2}\left(x_j - x_1^{p_j}\right)^2 p_j = 0.5\left(1 + 3\frac{j-2}{D-2}\right) g(\mathbf{x}) = 1 - f_1(\mathbf{x}) - f_2(\mathbf{x}) + \vert\sin(10\pi[f_1(\mathbf{x}) - f_2(\mathbf{x}) + 1])\vert$	$g(x) \le 0 0 \le x_i \le 1 J_1 = \{3,5,7,\cdots\} J_2 = \{2,4,6,\cdots\}$
	CF2	$f_1(\mathbf{x}) = x_1 + \frac{2}{\vert J_1\vert}\sum_{j\in J_1}\left(x_j - \sin\left(6\pi x_1 + \frac{j\pi}{D}\right)\right)^2 f_2(\mathbf{x}) = 1 - \sqrt{x_1} + \frac{2}{\vert J_2\vert}\sum_{j\in J_2}(x_j - \cos(6\pi x_1 + j\pi/D))^2 t(\mathbf{x}) = f_2(\mathbf{x}) + \sqrt{f_1(\mathbf{x})} - \sin(2\pi[\sqrt{f_1(\mathbf{x})} - f_2(\mathbf{x}) + 1]) - 1$	$t(\mathrm{x}) \ge 0 0 \le x_1 \le 1 J_1 = \{3,5,7,\cdots,\mathrm{D}\} J_2 = \{2,4,6,\cdots,\mathrm{D}\} -1 \le x_i \le 1 (i = 2,\cdots,D)$
	CF3	$f_1(\mathbf{x}) = x_1 + \frac{2}{\vert J_1\vert}\left[4\sum_{j\in J_1}(Y_j)^2 - 2\prod_{j\in J_1}\cos\left(\frac{20\pi Y_j}{\sqrt{j}}\right) + 2\right] f_2(\mathbf{x}) = 1 - (x_1)^2 + \frac{2}{\vert J_2\vert}\left[4\sum_{j\in J_2}(Y_j)^2 - 2\prod_{j\in J_2}\cos\left(\frac{20\pi Y_j}{\sqrt{j}}\right) + 2\right] Y_j = x_j - \sin\left(6\pi x_1 + \frac{j\pi}{D}\right) g(\mathbf{x}) = 1 - f_2(\mathbf{x}) - [f_1(\mathbf{x})]^2 + \sin\left(2\pi\left\{[f_1(\mathbf{x})]^2 - f_2(\mathbf{x}) + 1\right\}\right)$	$g(\mathbf{x}) \le 0 x_1 \in [0,1] x_{2..D} \in [-2,2]$

(continued on next page)

Table A1 (*continued*)

Benchmark	Test Function	Objectives (f_1 and f_2)	Constraints and Boundaries
	CF5	$f_1(\mathbf{x}) = x_1 + \sum_{j\in J_1} h_j f_2(\mathbf{x}) = (1-x_1) + \sum_{j\in J_2} h_j Y_j = \begin{cases} x_j - 0.8x_1\cos(6\pi x_1 + j\pi/D), & j\in J_1,\\ x_j - 0.8x_1\sin(6\pi x_1 + j\pi/D), & j\in J_2,\end{cases} g(\mathbf{x}) = -x_2 + 0.8x_1\sin\left(6\pi x_1 + \frac{2\pi}{D}\right) + 0.5x_1 - 0.25h_j = 2(Y_j)^2 - \cos(4\pi Y_j) + 1$	$g(\mathbf{x}) \le 0 x_1 \in [0,1]\, x_{2..D} \in [-2,2]$
	CF6	$f_1(\mathbf{x}) = x_1 + \sum_{j\in J_1}(Y_j)^2 f_2(\mathbf{x}) = (1-x_1)^2 + \sum_{j\in J_2}(Y_j)^2 Y_j = \begin{cases} x_j - 0.8x_1\cos\left(6\pi x_1 + \frac{j\pi}{D}\right), & j\in J_1,\\ x_j - 0.8x_1\sin\left(6\pi x_1 + \frac{j\pi}{D}\right), & j\in J_2\end{cases} g_1(\mathbf{x}) = -x_2 + 0.8x_1\sin\left(6\pi x_1 + \frac{2\pi}{D}\right) + \mathrm{sign}\left(0.5(1-x_1) - (1-x_1)^2\right)\sqrt{\lvert 0.5(1-x_1) - (1-x_1)^2 \rvert} g_2(\mathbf{x}) = -x_4 + 0.8x_1\sin\left(6\pi x_1 + \frac{4\pi}{D}\right) + \mathrm{sign}(0.25\sqrt{1-x_1} - 0.5(1-x_1))\sqrt{\lvert 0.25\sqrt{1-x_1} - 0.5(1-x_1)\rvert}$	$g_1(\mathbf{x}) \le 0 g_2(\mathbf{x}) \le 0 x_1 \in [0,1]\, x_{2..D} \in [-2,2]$
DTLZ	DTLZ1	$f_1(\mathbf{x}) = \frac{1}{2}(1+g(\mathbf{x}))x_1 f_2(\mathbf{x}) = \frac{1}{2}(1+g(\mathbf{x}))(1-x_1) g(\mathbf{x}) = 100\left(5 + \sum_{i=2}^{6}\left[(x_i - 0.5)^2 - \cos(20\pi(x_i - 0.5))\right]\right)$	$x_i \in [0,1]$
	DTLZ7	$f_1(\mathbf{x}) = x_1 f_2(\mathbf{x}) = 2(1+g(\mathbf{x})) - x_1(1+\sin(3\pi x_1)) g(\mathbf{x}) = 1 + \frac{9}{20}\sum_{i=2}^{21} x_i$	$0 \le x_i \le 1$
ZDT	ZDT1	$f_1(\mathbf{x}) = x_1 f_2(\mathbf{x}) = g(\mathbf{x})\left[1 - \sqrt{\frac{x_1}{g(\mathbf{x})}}\right] g(\mathbf{x}) = 1 + 9\cdot\mathrm{mean}(x_2,\cdots,x_{30})$	$0 \le x_i \le 1$
	ZDT2	$f_1(\mathbf{x}) = x_1 f_2(\mathbf{x}) = g(\mathbf{x})\left(1 - \left[\frac{x_1}{g(\mathbf{x})}\right]^2\right) = g(\mathbf{x}) - \frac{x_1^2}{g(\mathbf{x})} g(\mathbf{x}) = 1 + 9\cdot\mathrm{mean}(x_2,\cdots,x_{30})$	$0 \le x_i \le 1$
	ZDT3	$f_1(\mathbf{x}) = x_1 f_2(\mathbf{x}) = g(\mathbf{x})\left[1 - \sqrt{x_1/g(\mathbf{x})} - \frac{x_1}{g(\mathbf{x})}\sin(10\pi x_1)\right] g(\mathbf{x}) = 1 + 9\cdot\mathrm{mean}(x_2,\cdots,x_{30})$	$0 \le x_i \le 1$
	ZDT4	$f_1(\mathbf{x}) = x_1 f_2(\mathbf{x}) = g(\mathbf{x})\left[1 - \sqrt{\frac{x_1}{g(\mathbf{x})}}\right](\mathbf{x}) = 1 + 10(D-1) + \sum_{i=2}^{D}\left[x_i^2 - 10\cos(4\pi x_i)\right]$	$0 \le x_i \le 1$
	ZDT6	$f_1(\mathbf{x}) = 1 - \exp(-4x_1)\sin(6\pi x_1)^6 f_2(\mathbf{x}) = g(\mathbf{x})\left[1 - \left(\frac{f_1(\mathbf{x})}{g(\mathbf{x})}\right)^2\right] g(\mathbf{x}) = 1 + 9\left(\frac{1}{D-1}\sum_{i=2}^{D} x_i\right)^{0.25}$	$0 \le x_i \le 1$

Data availability

No data was used for the research described in the article.

References

Akram, M., & Bibi, R. (2023). Multi-criteria group decision-making based on an integrated PROMETHEE approach with 2-tuple linguistic Fermatean fuzzy sets. *Granular Computing, 8*, 917–941. https://doi.org/10.1007/s41066-022-00359-6

Başaran, H. H., & Tarhan, İ. (2022). Investigation of offshore wind characteristics for the northwest of Türkiye region by using multi-criteria decision-making method (MOORA). *Results in Engineering, 16*, Article 100757. https://doi.org/10.1016/j.rineng.2022.100757

Capossio, J. P., Fabani, M. P., Román, M. C., Zhang, X., Baeyens, J., Rodriguez, R., & Mazza, G. (2022). Zero-waste watermelon production through nontraditional rind flour: Multiobjective optimization of the fabrication process. *Processes,* 10(1984). https://doi.org/10.3390/pr10101984.

Chaudhuri, A., & Sahu, T. (2021). A hybrid feature selection method based on Binary Jaya algorithm for micro-array data classification. *Computers and Electrical Engineering, 90*. https://doi.org/10.1016/j.compeleceng.2020.106963

Chen, Y., & Zhou, A. (2022). Multiobjective portfolio optimization via Pareto front evolution. *Complex & Intelligent Systems, 8*(4301–4317). https://doi.org/10.1007/s40747-022-00715-8

Chiu, W.-Y., Yen, G. G., & Juan, T.-K. (2016). Minimum Manhattan distance approach to multiple criteria decision making in multiobjective optimization problems. *IEEE Transactions on Evolutionary Computation, 20*(6), 972–985. https://doi.org/10.1109/TEVC.2016.2564158

Cocchi, G., Lapucci, M., & Mansueto, P. (2021). Pareto front approximation through a multi-objective augmented Lagrangian method. *EURO Journal on Computational Optimization, 9*. https://doi.org/10.1016/j.ejco.2021.100008

Deb, K., Pratap, A., Agarwal, S., & Meyarivan, T. (2002). A fast and elitist multiobjective genetic algorithm: NSGA-II. *IEEE Transactions on Evolutionary Computation, 6*, 182–197. https://doi.org/10.1109/4235.996017

Deb, K., Thiele, L., Laumanns, M., & Zitzler, E. (2005). Scalable test problems for evolutionary multiobjective optimization. In *Evolutionary Multiobjective Optimization: Theoretical Advances and Applications* (pp. 105–145). Springer. https://doi.org/10.1007/1-84628-137-7_6.

Doke, A. B., Zolekar, R. B., Patel, H., & Das, S. (2021). Geospatial mapping of groundwater potential zones using multi-criteria decision-making AHP approach in a hardrock basaltic terrain in India. *Ecological Indicators, 127*, Article 107685. https://doi.org/10.1016/j.ecolind.2021.107685

Fernandez, E., Navarro, J., Solares, E., & Coello, C. (2018). A novel approach to select the best portfolio considering the preferences of the decision maker. *Swarm and Evolutionary Computation, 46*, 140–153. https://doi.org/10.1016/j.swevo.2019.02.002

Fernandez, E., Navarro, J., Solares, E., & Coello, C. (2020). Using evolutionary computation to infer the decision maker's preference model in the presence of imperfect knowledge: A case study in portfolio optimization. *Swarm and Evolutionary Computation, 54*. https://doi.org/10.1016/j.swevo.2020.100648

International Energy Agency & Centre for Climate Finance & Investment. (2020). Energy investing: Exploring risk and return in the capital markets (2nd ed.). International Energy Agency. Retrieved January 23, 2025, from https://www.iea.org/.

Jana, C., & Pal, M. (2021). A dynamical hybrid method to design a decision-making process based on GRA approach for multiple attributes problem. *Engineering Applications of Artificial Intelligence, 100*, Article 104203. https://doi.org/10.1016/j.engappai.2021.104203

Kaim, A., Cord, A., & Volk, M. (2018). A review of multi-criteria optimization techniques for agricultural land use allocation. *Environmental Modelling and Software, 105*, 79–93. https://doi.org/10.1016/j.envsoft.2018.03.031

Lazard. (2021). Lazard's levelized cost of energy analysis—Version 15.0. Lazard. Retrieved January 23, 2025, from https://lazard.com.

Li, H., Cao, Y., & Su, L. (2022). Pythagorean fuzzy multi-criteria decision-making approach based on Spearman rank correlation coefficient. *Soft Computing, 26*, 3001–3012. https://doi.org/10.1007/s00500-021-06615-2

Mazziotta, M., & Pareto, A. (2022). Normalization methods for spatio-temporal analysis of environmental performance: Revisiting the Min–Max method. *Environmetrics, 33*. https://doi.org/10.1002/env.2730

Nebro, A., Ruiz, A., Barba-González, C., García-Nieto, J., Luque, M., & Aldana-Montes, J. (2018). InDM2: Interactive dynamic multi-objective decision making using evolutionary algorithms. *Swarm and Evolutionary Computation, 40*, 184–195. https://doi.org/10.1016/j.swevo.2018.02.004

Petchrompo, S., & Parlikad, A. (2019). A review of asset management literature on multi-asset systems. *Reliability Engineering and System Safety, 181*, 181–201. https://doi.org/10.1016/j.ress.2018.09.009

Petchrompo, S., Coit, D., Brintrup, A., Wannakrairot, A., & Parlikad, A. (2022). A review of Pareto pruning methods for multi-objective optimization. *Computers and Industrial Engineering, 167*. https://doi.org/10.1016/j.cie.2022.108022

Pham-Gia, T., & Hung, T. L. (2001). The mean and median absolute deviations. *Mathematical and Computer Modelling, 34*, 921–936. https://doi.org/10.1016/S0895-7177(01)00109-1

Syan, S., & Ramsoobag, G. (2019). Maintenance applications of multi-criteria optimization: A review. *Reliability Engineering and System Safety, 190*. https://doi.org/10.1016/j.ress.2019.106520

Taherdoost, H., & Madanchian, M. (2023). A comprehensive overview of the ELECTRE method in multi-criteria decision-making. *Journal of Management Science & Engineering Research, 6*(2), 5–16. https://doi.org/10.30564/jmser.v6i2.5637

Taherdoost, H., & Mohebi, A. (2024). A comprehensive guide to the COPRAS method for multi-criteria decision making. *Journal of Management Science & Engineering Research, 7*(2), 1–14. https://doi.org/10.30564/jmser.v7i2.6280

Tian, Y., Cheng, R., Zhang, X., Li, M., & Jin, Y. (2019). Diversity assessment of multi-objective evolutionary algorithms: Performance metric and benchmark problems. *IEEE Computational Intelligence Magazine*. https://doi.org/10.1109/MCI.2019.2919398

Trung, D. D. (2021). Application of TOPSIS and PIV methods for multi-criteria decision making in hard turning process. *Journal of Machine Engineering, 21*(4), 57–71. https://doi.org/10.36897/jme/142599

Vaid, S. K., Vaid, G., Kaur, S., Kumar, R., & Sidhu, M. S. (2022). Application of multi-criteria decision-making theory with VIKOR-WASPAS-Entropy methods: A case study of silent Genset. *Materials Today: Proceedings, 50*, 2416–2423. https://doi.org/10.1016/j.matpr.2021.10.259

Wang, Q., & Jia, X. (2020). Multi-objective optimization of CFRP drilling parameters with a hybrid method integrating the ANN, NSGA-II, and fuzzy C-means. *Composite Structures, 235*. https://doi.org/10.1016/j.compstruct.2019.111803

Wang, S., Wu, F., Takyi-Aninakwa, P., Fernandez, C., Stroe, D.-I., & Huang, Q. (2023). Improved singular filtering-Gaussian process regression-long short-term memory model for whole-life-cycle remaining capacity estimation of lithium-ion batteries adaptive to fast aging and multi-current variations. *Energy, 284*, Article 128677. https://doi.org/10.1016/j.energy.2023.128677

Yahoo Finance. (n.d.). Historical stock prices for Tesla Inc. (TSLA), Amazon Inc. (AMZN), and Apple Inc. (AAPL). Retrieved January 22, 2025, from https://finance.yahoo.com.

Yu, P. L. (1973). A class of solutions for group decision problems. *Management Science, 19*, 936–946. https://doi.org/10.1287/mnsc.19.8.936

Zavadskas, E. K., Kaklauskas, A., & Šarka, V. (1994). The new method of multicriteria complex proportional assessment of projects. *Technological and Economic Development of Economy*, 131–139. https://etalpykla.vilniustech.lt/handle/123456789/111916.

Zhang, Q., Zhou, A., Zhao, S., Suganthan, P. N., Liu, W., & Tiwari, S. (2009). Multiobjective optimization test instances for the CEC 2009 special session and competition. School of CS & EE, University of Essex, Working Report CES-487. https://www.al-roomi.org/multimedia/CEC_Database/CEC2009/MultiObjectiveEA/CEC2009_MultiObjectiveEA_TechnicalReport.pdf.

Zitzler, E., Deb, K., & Thiele, L. (2000). Comparison of multiobjective evolutionary algorithms: Empirical results. *Evolutionary Computation, 173–195*. https://doi.org/10.1162/106365600568202